Protonic conductivity and ferroelastic instability in triammonium hydrogen disulphate: a dielectric and neutron diffraction study

1998 J. Phys.: Condens. Matter 10 3019

(http://iopscience.iop.org/0953-8984/10/13/018)

J. Phys.: Condens. Matter **10** (1998) 3019–3027. Printed in the UK PII: S0953-8984(98)89086-3

Protonic conductivity and ferroelastic instability in triammonium hydrogen disulphate: a dielectric and neutron diffraction study

L Schwalowsky†, V Vinnichenko‡, A Baranov‡, U Bismayer†, B Merinov‡ and G Eckold§

† Mineralogisch-Petrographisches Institut, Universität Hamburg, Grindelallee 48, D-20146 Hamburg, Germany

‡ Institute of Crystallography, Russian Academy of Sciences, Leninsky Prospekt 59, 11733 Moscow, Russia

§ Institut für Physikalische Chemie, Universität Göttingen, Tammannstrasse 6, D-37077 Göttingen, Germany

Received 10 November 1997, in final form 16 January 1998

Abstract. The protonic conductivity of $(NH_4)_3H(SO_4)_2$ has been measured using the complex-admittance method in the frequency range 30 Hz–200 MHz and the temperature interval 290–500 K covering both the ferroelastic ($A2/a$) and the paraelastic ($R\bar{3}m$) phases. The dc conductivity shows quasi-two-dimensional behaviour and in the trigonal paraelastic phase its values in the (001) plane are typically super-protonic ($10^{-2} \leqslant \sigma_{(001)} \leqslant 10^{-1}$ S cm^{-1}) with low activation enthalpy $H^{a}_{(001)} = 0.24$ eV. The temperature dependence of the monoclinic superstructure reflection 120 has been studied using elastic neutron diffraction. It was found that the observed anomalies of the macroscopic and microscopic quantities, such as the morphic birefringence and the high-frequency dielectric constant on the one hand and the diffusion proton dynamics as well as the integrated intensity of the reflection 120 on the other hand, show pronounced differences in their temperature evolution below the ferroelastic phase transition temperature. The neutron scattering results as well as the dielectric measurements indicate precursor effects above T_c. The results are discussed on the basis of a phenomenological two-order-parameter model for the D^5_{3d}–C^6_{2h} ferroelastic phase transition. It is argued that properties which originate from the disorder of the oxygen and proton subsystem can be described by irreducible representations of the wave vector at the Γ point and the L point of the Brillouin zone, while properties which originate from displacements of the heavy atoms (the displacement mode) are solely described by the wave vector at the L point of the Brillouin zone of the paraphase.

1. Introduction

Triammonium hydrogen disulphate $(NH_4)_3H(SO_4)_2$ belongs to the well known family of ferroelastic materials with the general formula $M_3H(AO_4)_2$ (M = K, Rb, Cs, NH_4; A = S, Se). Above room temperature, crystals of this family undergo an improper ferroelastic phase transition with the symmetry change $A2/a$ (C^6_{2h})–$R\bar{3}m$ (D^5_{3d}) [1–4]. From the symmetry point of view this phase transition is isomorphous with the ferroelastic phase transition in crystals of the lead-phosphate-type compounds $Pb_3(BO_4)_2$ where B = P, As, V [5–7]. The crystal structures of these compounds as well as the substructure of the heavy atoms in $M_3H(AO_4)_2$ belong to the family of the palmierite-type structure. The structural

0953-8984/98/133019+09$19.50

differences are due to the presence of protons in $M_3H(AO_4)_2$. In the ferroelastic phase ($A2/a$) the protons form strong symmetric hydrogen bonds with lengths of 2.55 Å–2.7 Å. The centres of the hydrogen bonds correspond to the 2h Wyckoff positions. Hence, the location of the hydrogen bonds in the ferroelastic phase is fixed to a single site by the crystal symmetry. In the trigonal paraelastic phase, however, the centres of three H bonds per unit cell are distributed over the 9e positions with occupational probability 1/3, forming a dynamically disordered hydrogen bond network (DDHBN) in the (001) plane. Because of this kind of proton disorder, the protons can migrate throughout the crystal volume with a low activation energy, giving rise to high protonic conductivity in $M_3H(AO_4)_2$ [8]. In contrast to the lead-phosphate-type crystals, for which the ferroelastic phase transition in a single domain is purely displacive in character (precursor phenomena occur above T_c), the isomorphous phase transition in $M_3H(AO_4)_2$ is a combination of displacive and order–disorder contributions in the ferrophase. This effect leads to drastic differences in the physical properties of both systems. For example, the transition entropies of the ferroelastic phase transition in the $M_3H(AO_4)_2$ crystals, $10 \leqslant S \leqslant 10.3$ J mol^{-1} K^{-1} [9–11], are larger than those of $Pb_3(BO_4)_2$ ($S = 6.7$ J mol^{-1} K^{-1} [12]). Moreover the coercive stress of the domain switching in $M_3H(AO_4)_2$ is much larger than that for crystals of the $Pb_3(BO_4)_2$ system [13, 14]. However, the most striking differences are observed in the transport properties [8, 15]. Therefore, it is of great importance to clarify the interplay between the order parameter, the occupational probability of acid protons and the protonic conductivity in $M_3H(AO_4)_2$. It was noted earlier [16] that the best-known super-ionic phase transitions are of the martensitic or the ferroelastic type. A first interpretation of the anomalous behaviour of the ionic conductivity at a ferroelastic phase transition has been given on the basis of the Landau theory in [2, 16], where an empirical relation between the activation energy of ionic conductivity and the order parameter has been determined.

In the present work an experimental study of the thermal evolution of the protonic conductivity, the high-frequency dielectric constant and the scattering intensity of a superlattice reflection in $(NH_4)_3H(SO_4)_2$ (letovicite) has been carried out. The results of this study as well as the recently obtained birefringence data [13] are analysed on the basis of a theoretical model which relates the anomalous behaviour of the above-mentioned physical properties to two order parameters. The different order parameters describe the change of the average occupancy of the hydrogen bond positions as well as the spontaneous deformation.

2. Experimental details

Isometric letovicite single crystals were grown from saturated water solutions by slow evaporation in a temperature-controlled chamber. The conductivity and capacity measurements were carried out in the temperature interval 290 K–500 K and the frequency range 30 Hz–200 MHz using ac Ando-Electric TR-10C and high-frequency VM-431E bridges. The prepared samples had a plate-like form of $6 \times 6 \times 0.1$ mm^3 with faces perpendicular to the a-, b- and c-axes (the orthorhombic setting was used). Silver paste served as the electrodes.

The neutron measurements were performed using the triple-axis spectrometer UNIDAS at the research reactor FRJ-2 in Jülich, Germany. The thermal evolution of the diffraction profile of the monoclinic 120 superlattice reflection was recorded using a wavelength of 2.36 Å. The crystal ($18 \times 6 \times 1$ mm^3) was mounted on an aluminium block with its a^*b^*-plane horizontally aligned and enclosed in an aluminium cylinder filled with He gas. The

heating was performed via the metal block and the gas atmosphere. The temperature was controlled with an accuracy of ± 0.06 K.

Table 1. The activation enthalpy H_i^a and the prefactor A_i in equation (1).

Phase	Axis	A (S cm^{-1} K)	H^a (eV)
Monoclinic	*a*	1.1×10^6	0.51
Monoclinic	*b*	1.9×10^6	0.52
Monoclinic	*c*	$7.1 \times 10^{10*}$	1.01
Trigonal	*a*	4.7×10^3	0.23
Trigonal	*b*	4.9×10^3	0.23
Trigonal	*c*	1.3×10^4	0.42

* The value corresponding to the temperature interval 290 K–360 K.

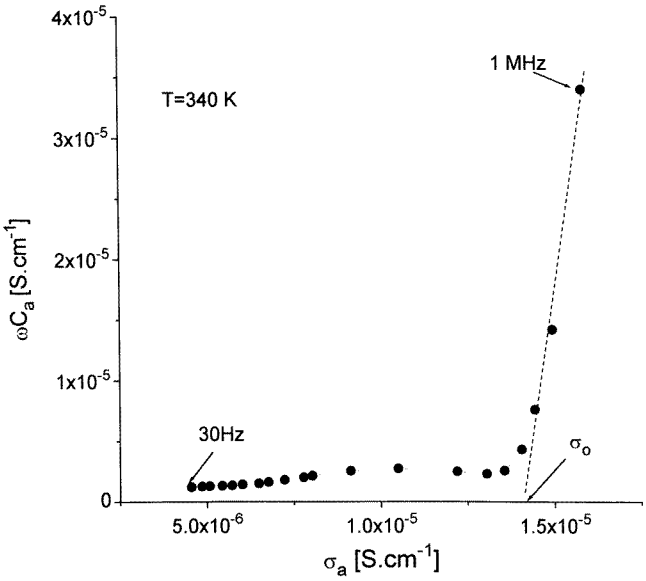

Figure 1. Bulk dc conductivities calculated from the frequency dependencies of the complex admittance $\sigma^*(\omega) = \sigma'(\omega) + \mathrm{i}\sigma''(\omega)$. The low-frequency part of the admittance (the lower arc of the circle) corresponds to the electrode and the interfacial relaxation polarization. The high-frequency part (the inclined line) corresponds to the bulk frequency conductivity $\sigma^*_{\mathrm{bulk}}(\omega)$.

3. Results

The bulk dc conductivities were calculated from the frequency dependencies of the complex admittance $\sigma^*(\omega) = \sigma(\omega) + \mathrm{i}\omega C(\omega)$. Their values are plotted in the complex plane (figure 1). In figure 1 the low-frequency part of the admittance (the lower arc of the circle) corresponds to the electrode and the interfacial relaxation polarization, while the high-frequency part (the inclined line) corresponds to the bulk frequency-dependent conductivity $\sigma^*_{\mathrm{bulk}}(\omega)$. The bulk dc conductivity σ^{dc} was determined by extrapolation of the $\sigma^*_{\mathrm{bulk}}(\omega)$ data to $\omega = 0$. Figure 2 shows an Arrhenius plot of the thermal evolution of the dc bulk

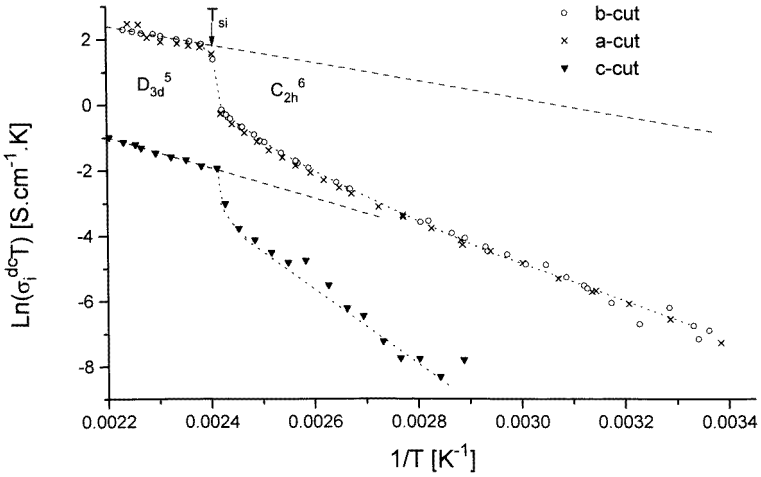

Figure 2. An arrhenius plot of the thermal variation of the bulk dc conductivity σ_i^{dc} in different crystallographic directions. Dashed lines correspond to fits obtained using equation (1). Dotted lines correspond to fits based on equation (3). The parameters are given in table 1.

conductivity σ_i^{dc} in different crystallographic directions in letovicite. The strong anisotropy of the conductivity, $\sigma_a^{\mathrm{dc}} \cong \sigma_b^{\mathrm{dc}} \gg \sigma_c^{\mathrm{dc}}$, in both the ferrophase and the paraphases clearly reflects the two dimensionality of the most favourable proton migration pathways, which agrees well with the layer structure of letovicite as well as with the small ferroelastic distortions $u_{\mathrm{s}} \leqslant 10^{-3}$ of the monoclinic ferrophase [13]. The ferroelastic phase transition is accompanied by an abrupt change of the conductivity and its activation enthalpy H_i^{a}. At $T \geqslant T_{\mathrm{c}}$ the conductivity in the (001) plane of the trigonal paraelastic phase is typically super-ionic, $\sigma_a^{\mathrm{dc}} = \sigma_b^{\mathrm{dc}} \cong 10^{-2}$ S cm^{-1}, and tends to increase to 10^{-1} S cm^{-1} on approaching the decomposition point $T_{\mathrm{d}} \approx 500$ K. The values of H_i^{a} and the prefactor A_i in the Arrhenius law

$$\sigma_i^{\mathrm{dc}} T = A_i \exp(-H_i^{\mathrm{a}}/kT) \tag{1}$$

are characteristic for super-ionic crystals (see table 1).

It should be noted that the temperature dependencies of σ_c^{dc} which are shown in figure 2 are close to those reported in [17], where the measurements were carried out at a dc current which is not such as to allow one to disregard the contribution of the electrode polarization. On the other hand the $\sigma_i^{\mathrm{dc}}(T)$ variation as well as the values of H_i^{a} and A_i obtained in this work are in excellent agreement with those obtained for other crystals of the $M_3H(AO_4)_2$ family [8]. This is in accordance with the general nature of super-protonic phase transitions and structural mechanisms of proton transport in these compounds. As mentioned above, in the (001) plane of the paraelastic super-protonic phase, the hydrogen bonds are dynamically distributed over structurally and energetically equivalent proton sites with occupation probability 1/3. Therefore, in this plane only the enthalpy of the proton migration $H_{a,b}^{\mathrm{m}}$ contributes to the experimental values of the activation enthalpy $H_{a,b}^{\mathrm{a}}$. In other words, the protonic conductivity in the (001) plane of the paraelastic phase is a property of the perfect-crystal lattice but it is not a property of the point defects. However, below T_{c} the average proton occupation probability is changed, being a function of the order parameter. Only a third of the available hydrogen bond sites of the trigonal phase correspond to the regular hydrogen bond sites of the ferrophase, while the remaining sites correspond

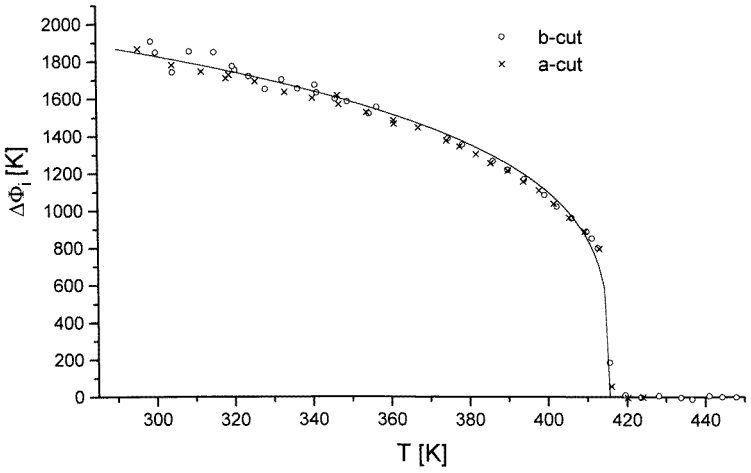

Figure 3. The thermal evolution of the activation thermodynamic potentials $\Delta\Phi_a^{\mathrm{d}}$ and $\Delta\Phi_b^{\mathrm{d}}$ calculated from the experimental temperature dependencies of the dc conductivity following equation (2). The continuous line displays the fit obtained according to equation (4); $T_{\mathrm{c}} = 415.6$ K, $2\beta' = 0.26$.

to interstitial positions. This means that in the ferroelastic phase, proton hopping between the adjusted hydrogen bond sites involves the formation of proton defects. As a result, the activation enthalpy of the conductivity increases compared with that of the paraelastic phase by the value $\Delta\Phi^{\mathrm{d}}$:

$$\Delta\Phi^{\mathrm{d}} = \Delta\Phi^{0} - \Delta\Phi^{\mathrm{e}} \tag{2}$$

where $\Delta\Phi^{0}$ and $\Delta\Phi^{\mathrm{e}}$ are thermodynamic potentials of the crystal in the ground state (in which all protons occupy regular sites) and the state in which the protons were thermally excited to occupy interstitial positions. The potential $\Delta\Phi^{\mathrm{d}}$, being a function of the proton occupational probability, is also a function of the lattice distortion at the phase transition and consequently a the function of the order parameter. Therefore, below T_{c} the conductivity in different crystallographic directions σ_i^{dc} can be described by the expression

$$\sigma_i^{\mathrm{dc}} T = A_i^{\mathrm{m}} \exp[-H_i^{\mathrm{m}} - \Delta\Phi_i^{\mathrm{d}}(\eta)]/kT \tag{3}$$

where A_i^{m} and H_i^{m} are parameters of equation (1) for the disordered paraelastic phase. The thermal evolution of $\Delta\Phi_a^{\mathrm{d}}$ and $\Delta\Phi_b^{\mathrm{d}}$ obtained by subtraction of the monoclinic conductivity data from the extrapolated high-temperature data is displayed in figure 3. It should be noted that no discontinuities occur within the experimental error, and the excess ($\Delta\Phi_i^{\mathrm{d}}$) data can be fitted by a simple power law with an effective critical exponent according to

$$\Delta\Phi_a^{\mathrm{d}} \cong \Delta\Phi_a^{\mathrm{d}} \propto (T_{\mathrm{c}} - T)^{2\beta'} \tag{4}$$

where $T_{\mathrm{c}} = 415.6$ K and $2\beta' = 0.26$.

The temperature dependency of ε', the real part of the complex dielectric constant measured at frequencies which are much higher than the characteristic frequency of the long-range proton diffusion, shows a quite different behaviour (figure 4). The sharp anomaly of $\varepsilon_{\mathrm{c}}'(T)$ at the phase transition point is characteristic of a first-order phase transition rather than a second-order one. However, the temperature hysteresis does not exceed the experimental error of ± 0.1 K. The behaviour of ε' agrees well with that of the morphic birefringence Δn along the direction which becomes $[001]_{\mathrm{hex}}$ in the paraphase [13].

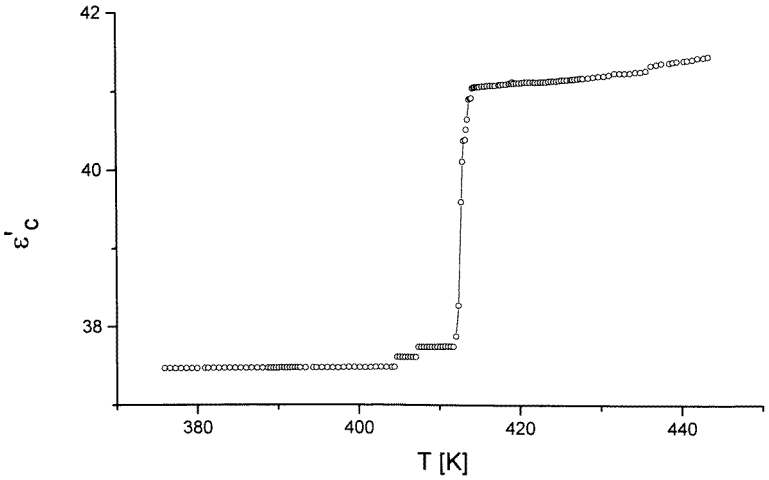

Figure 4. The temperature evolution of ε'_c measured at the frequency 100 MHz.

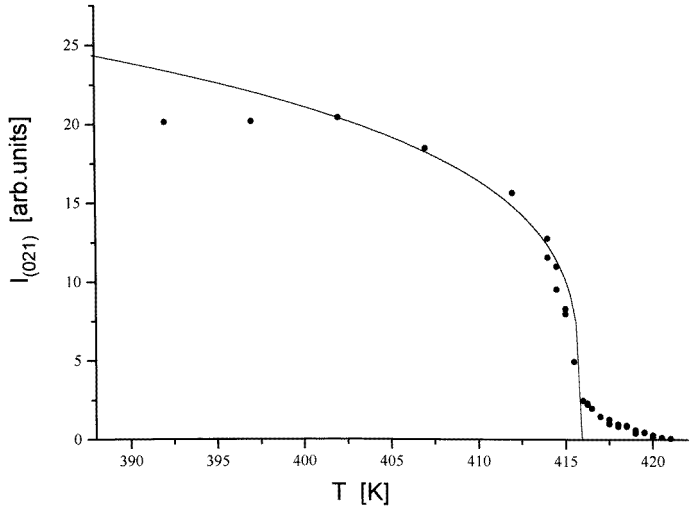

Figure 5. The thermal evolution of the 120 reflection measured by means of neutron scattering. The integrated intensity of this reflection decreases smoothly with a tail above T_c (415.6 K). The reflection remains visible up to $T = T_c + 6$ K. The solid line corresponds to a fit to equation (5).

Let us now compare the thermal evolution of the 120 reflection measured by means of neutron scattering on approaching T_c. The integrated intensity of this reflection decreases smoothly (figure 5). However, the reflection remains clearly visible up to $T = T_c + 6$ K. In the temperature range $T_c - 15\ \text{K} \leqslant T \leqslant T_c$ a best fit of $I_{(120)}(T)$ leads to

$$I_{(120)} \propto (T - T_c)^{0.25} \tag{5}$$

which agrees well with the thermal variation of $\Delta\Phi_i^d$ and the corresponding effective exponent (equation (4)).

Taking into account that in a general case $\Delta\Phi_a^d$ and $I_{(120)}$, as well as the excess values of ε' and the morphic birefringence Δn are, in the lowest order, proportional to the square

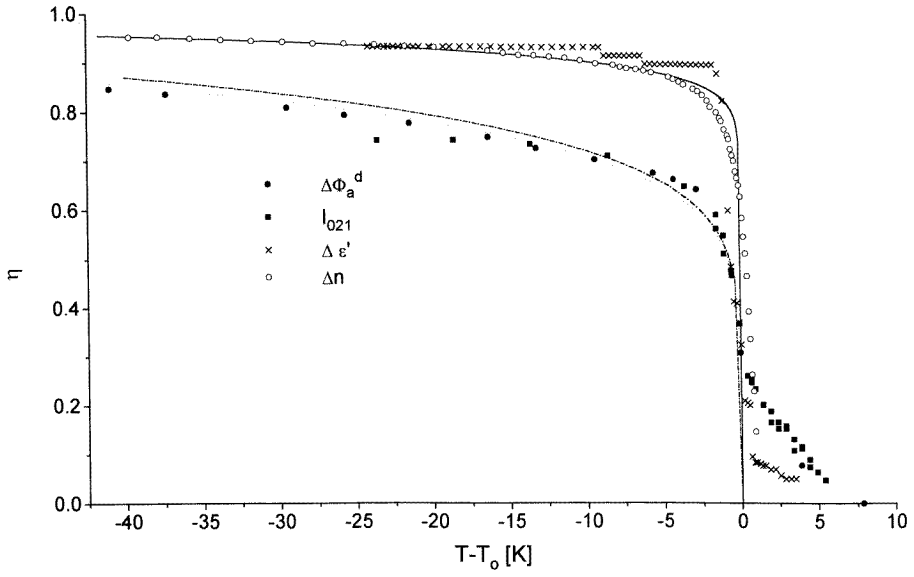

Figure 6. The square roots of normalized $\Delta\Phi_a^{\mathrm{d}}$, $I_{(120)}$, $\varepsilon_{\mathrm{c}}'$ and Δn versus temperature. The birefringence data are taken from Schwalowsky *et al* [13]. The temperature evolution of $\Delta\Phi_i^{\mathrm{d}}$ and $I_{(120)}$ clearly deviate from ε' and Δn. Excess values above T_{c} occur only for $I_{(120)}$ and ε'. The lines correspond to fits based on a simple power law. For a description of the different effective critical exponents, see the text.

of the order parameter η, the square roots of these functions were plotted as a function of temperature in figure 6. The birefringence data were taken from [13]. Please note that different effective exponents result from best fits to the simple power law, because Schwalowsky *et al* [13] used a theoretical approach related to a Slater instability [18] which describes the rapid order parameter saturation yielding $\beta' = 0.04$. The smoothly decreasing values of $\Delta\Phi_a^{\mathrm{d}}$ and $I_{(120)}$ are instead described by a power law that yields $\beta' = 0.13$. Hence, it can be seen that the temperature evolutions of $\Delta\Phi_a^{\mathrm{d}}$ and $I_{(120)}$ on one hand and ε' and Δn on the other hand differ considerably. No excess values occur above T_{c} for ε' and Δn.

4. Discussion

The results lead to the assumption that the ferroelastic phase transition in letovicite can be described by two order parameters with different temperature dependencies. Their contributions to the temperature evolution of the properties on different length scales deviate strongly. A self-consistent thermodynamic model for describing D_{3d}^5–C_{2h}^6 phase transitions in terms of two order parameters has been formulated in [19, 21]. From the symmetry point of view this phase transition is an improper ferroelastic one and is induced by the irreducible (IR) representation of the group of the wave vector $\boldsymbol{G}_{K_4}$ (the L point of the Brillouin zone of the paraphase) [5, 19]. However, as mentioned above, the lowering of the symmetry in a $(NH_4)_3H(SO_4)_2$ crystal is also accompanied by a change in the occupational probability of the hydrogen bond sites: in the trigonal phase two protons are statistically distributed over six structurally equivalent hydrogen bond sites in a primitive unit cell, while in the monoclinic phase only two of them are occupied by protons. As was shown in

references [19, 20], the IR corresponding to $\boldsymbol{G}_{\boldsymbol{K}_4}$ cannot correctly describe the change of the occupational probability of the hydrogen bond sites at the D_{3d}^5–C_{2h}^6 phase transition: two sites are occupied by hydrogen (black sites), two sites are empty (white sites) and two sites remain insensitive to the symmetry of the wave vector $\boldsymbol{G}_{\boldsymbol{K}_4}$ (grey sites). Similar difficulties as regards symmetry descriptions of order–disorder phase transitions were encountered for the Nb–H and Ta–H alloys [21]. To describe the proton ordering, a separation of the six proton positions in the trigonal system into two orbits had to be considered. This led to the procedure described by Salejda and Dzhavadov [19, 20] and to the avoidance of the grey positions in $Rb_3H(SeO_4)_2$. The authors showed that the D_{3d}^5–C_{2h}^6 phase transition is induced by irreducible representations corresponding to the wave vectors $\boldsymbol{G}_{\boldsymbol{K}_4=\boldsymbol{b}_{3/2}}$ (the L point) and $\boldsymbol{G}_{\boldsymbol{K}=\boldsymbol{0}}$ (the Γ point). A free-energy expression based on the molecular-field approximation which correctly describes the proton ordering was obtained [20] in the form

$$F_{\mathrm{MFA}} = -T \ln \mathcal{Z} + \gamma \eta_{\Gamma}^2 + \gamma_1 \eta_{\mathrm{L}}^2 \tag{6}$$

where γ and γ_1 are molecular-field parameters connected with the long-range interactions of protons and $\mathcal{Z}$ is the quantum partition function correlated with the configurations of protons which are described in detail in [20]. The average occupancy of the hydrogen bond sites is in fact a function of both order parameters, η_{L} and η_{Γ}, corresponding to the $\boldsymbol{G}_{\boldsymbol{K}_4=\boldsymbol{b}_{3/2}}$ and $\boldsymbol{G}_{\boldsymbol{K}=\boldsymbol{0}}$ wave vectors, respectively. Moreover, the influence of η_{L} on the degree of proton disorder is much stronger than that of η_{Γ} [19, 20]. Hence, the conductivity and the neutron scattering integrated intensity of the 120 reflection are highly sensitive to the temperature evolution of the order parameter η_{L}, in contrast to the morphic birefringence and the high-frequency dielectric constant which are perfectly described by the long-ranging spontaneous strain that transforms according to the basis function of η_{Γ}, which is E_g. Hence, neutron scattering and conduction phenomena clearly display proton ordering. The observed precursor phenomena above the ferroelastic transition point (figures 5, 6) will be studied in detail in a separate work.

Acknowledgments

The authors wish to thank V V Dolbinina for providing some of the crystals. Financial support provided by the Volkswagen Stiftung is gratefully acknowledged. UB is grateful to the DFG for support of part of the work.

References

[1] Suzuki S and Makita Y 1978 The crystal structure of triammonium hydrogen disulphate $(NH_4)_3H(SO_4)_2$ *Acta Crystallogr.* B **34** 732

[2] Baranov A I, Makarova I P, Muradyan L A, Tregubchenko A V, Shuvalov L A and Simonov V I 1987 Phase transitions and protonic conductivity in $Rb_3H(SeO_4)$ crystals *Sov. Phys.–Crystallogr.* **32** 400

[3] Merinov B V, Baranov A I and Shuvalov L A 1990 Crystal structure and mechanism of protonic conductivity of the superionic phase of $Cs_3H(SeO_4)_2$ *Sov. Phys.–Crystallogr.* **35** 200

[4] Merinov B V, Bolotina N B, Baranov A I and Shuvalov L A 1991 Crystal structure of ferroelastic phase II of $Cs_3H(SeO_4)_2$ *Sov. Phys.–Crystallogr.* **36** 639

[5] Torres J 1975 Symetrie du parametre d'ordre de la transition de phase ferroelastique du phosphate de plomb *Phys. Status Solidi* b **71** 141

[6] Bismayer U and Salje E 1981 Ferroelastic phases in $Pb_3(PO_4)_2$–$Pb_3(AsO_4)_2$; x-ray and optical experiments *Acta Crystallogr.* A **37** 145

[7] Paulmann C, Bismayer U and Aroyo M 1998 Precursors in lead phosphate-type ferroelastics: diffuse x-ray scattering, group theory and modelling *Phase Transitions* at press

[8] Baranov A I, Merinov B V, Tregubchenko A V, Khiznichenko V P, Shuvalov L A and Schagina NM 1989 Fast proton transport in crystals with a dynamically disordered hydrogen bond network *Solid State Ion.* **36** 279

[9] Suzuki S, Oshino Y, Gesi K and Makita Y 1979 Calorimetric study on phase transitions in $(NH_4)_3H(SO_4)_2$ *J. Phys. Soc. Japan* **47** 878

[10] Osaka T, Sato T and Makita Y 1984 Thermal and dielectric studies of $(NH_4)_3H(SeO_4)_2$ and isotope effect *Ferroelectrics* **55** 283

[11] Dilanyan P A, Sinitsyn V V, Shekhtman V Sh, Baranov A I and Shuvalov LA 1994 The discovery of an intermediate phase between the low-conducting and super-protonic phases in $Rb_3H(SeO_4)_2$ *Crystallogr. Rep.* **39** 428

[12] Salje E and Wruck B 1983 Specific-heat measurements and critical exponents of the ferroelastic phase transition in $Pb_3(PO_4)_2$ and $Pb_3(P_{1-x}As_xO_4)_2$ *Phys. Rev.* B **28** 6510

[13] Schwalowsky L, Bismayer U and Lippmann T 1996 The improper ferroelastic phase transition of letovicite, $(NH_4)_3H(SO_4)_2$: an optical birefringence, x-ray diffraction and Raman spectroscopic study *Phase Transitions* **59** 61

[14] Bismayer U, Salje E and Joffrin C 1982 Reinvestigation of the stepwise character of the ferroelastic phase transition in lead phosphate–arsenate, $Pb_3(PO_4)_2$–$Pb_3(AsO_4)_2$ *J. Physique* **43** 1379

[15] Wruck B, Bismayer U and Salje E 1981 Dielectric properties of $Pb_3(PO_4)_2$–$Pb_3(AsO_4)_2$ *Mater. Res. Bull.* **16** 251

[16] Baranov A I 1987 Anomalies of protonic conductivity at structural phase transitions in hydrogen-bonded crystals *Izv. Akad. Nauk SSSR Ser. Fiz.* **51** 2146

[17] Ramasastry C and Subna R K 1981 Electrical conduction in $Na_3H(SO_4)_2$ and $(NH_4)_3H(SO_4)_2$ *J. Mater. Sci.* **16** 2011

[18] Bastie P, Vallade M, Vettier C, Zeyen C M E and Meister H 1981 Neutron diffractometry investigation of the tricritical point of KH_2PO_4 *J. Physique* **42** 445

[19] Salejda W and Dzhavadov N A 1990 Phase transition in $Rb_3H(SeO_4)_2$-type crystals. I. The symmetry analysis of proton ordering *Phys. Status Solidi* b **158** 119

[20] Salejda W and Dzhavadov N A 1990 Phase transition in $Rb_3H(SeO_4)_2$-type crystals. II. The molecular field approximation *Phys. Status Solidi* b **158** 475

[21] Izyumov Yu A and Syromyatnikov V N 1984 *Phase Transitions and the Symmetry of Crystals* (Moscow: Nauka)